Characterization of Epitaxial Heavily Doped Silicon Regions Formed by Hot-Wire Chemical Vapor Deposition Using Micro-Raman and Microphotoluminescence Spectroscopy

Tasmiat Rahman , Hieu T. Nguyen , Antulio Tarazona, Jingxing Shi, Young-Joon Han , Evan Franklin, Daniel Macdonald, and Stuart A. Boden

Abstract—We report on the characterization of heavily boron doped epitaxial silicon regions grown in a hot-wire chemical vapor deposition tool, using micro-Raman and photoluminescence spectroscopy. In particular, the use of this approach for emitter fabrication in an interdigitated back contact silicon solar cell is studied, by analyzing its suitability concerning selective growth, uniformity, anneal time, and luminescent defects. We show that by reducing the silane flow rate, both the required postanneal time and intensity of defect luminescence are reduced. Furthermore, we show that selective area growth does not affect either the quality of the films or the sharpness of the resulting lateral doping profile. The uniformity of the doping is shown to be better than that achieved using laser doping.

Index Terms—Epitaxy, hot-wire chemical vapor deposition (HWCVD), laser doping, silicon, spectral photoluminescence (PL).

I. INTRODUCTION

INTERDIGITATED back contact (IBC) architectures are amongst the highest efficiency silicon solar technologies. Recently, a record breaking efficiency of 26.7% was achieved by Kaneka Corporation using an IBC approach [1]. The advantage of a back-contact architecture is the elimination of a metal grid shading at the front surface, which leads to increased short circuit currents. Furthermore, unlike conventional cell designs, with the IBC architecture, antireflective and light trapping structures such as black-Si [2], [3], can be incorporated into the front surface without the need to be compatible with contacts or a p-n junction near to the surface.

Various approaches exist for forming the p- and n- type selective contact regions in an IBC solar cell, including high temperature diffusions with gaseous dopant sources of BBr_3 and $POCl_3$ [4], [5], as well as ion implantation [6]. Formation of localized IBC solar cell contacts via laser doping have, meanwhile, been demonstrated using both green and UV pulsed nanosecond laser sources, and dopant precursors [7], [8]. In this paper, we explore the use of selectively grown epitaxial emitters, which have advantages over normal diffused junctions including potentially shorter processing times, lower thermal budgets, and more control over doping profiles. Recently, several groups have utilized epitaxial emitters for photovoltaics (PV), including Recaman Payo *et al.*, who used boron-doped epitaxy by LPCVD for an IBC solar cell [9], and Rachow *et al.* who produced PERL devices using APCVD to form the phosphorus-doped epitaxial emitter [10]. Here, we study epitaxially-grown emitters using a commercial hot-wire chemical vapor deposition (HWCVD) system, which provides a scalable route to lower manufacturing costs compared with other techniques. We recently reported high-quality junction formation with such doped films, with the potential for making high-efficiency solar cells [11]. For this paper, we have undertaken a study to understand the influence of reduced silane rates, annealing times, and selective area growth on doping quality and luminescent defects. To characterize these parameters effectively, photoluminescence (PL) imaging, micro-PL spectroscopy and micro-Raman spectroscopy are used.

PL techniques have been demonstrated to be powerful tools for material and device characterization in silicon PV [12]–[14]. PL imaging reveals the spatial distribution of radiative recombination in silicon wafers and solar cells, with dark areas (lower PL intensities) that indicate high levels of nonradiative, defect-induced recombination. Spectrally-resolved PL can offer further insights, providing information on material properties including

T. Rahman, J. Shi, and S. A. Boden are with the Department of Electronics and Computer Science, University of Southampton, Southampton SO17 1BJ, U.K. (e-mail: t.rahman@soton.ac.uk; js5e10@ecs.soton.ac.uk; sb1@ecs.soton.ac.uk).

H. T. Nguyen, Y.-J. Han, and D. Macdonald are with the Research School of Engineering, Australian National University, Canberra ACT 2601, Australia (e-mail: hieu.nguyen@anu.edu.au; young.han@anu.edu.au; daniel.macdonald@anu.edu.au).

A. Tarazona is with the Optoelectronics Research Centre, University of Southampton, Southampton SO17 1BJ, U.K. (e-mail: at2@ecs.soton.ac.uk).

E. Franklin is with the School of Engineering, University of Tasmania, Hobart, TAS 7001, Australia (e-mail: evan.franklin@anu.edu.au).

absorption [15]–[17] and recombination coefficients [16], [18], [19], light trapping [20], and minority carrier diffusion lengths and lifetimes [21]–[25]. Recently, with the advent of micro-PL tools equipped with a confocal microscope, microstructures in silicon wafers and solar cells can be investigated with very high spatial resolution, enabling the study of dislocation clusters [26], [27], grain boundaries [28], metal precipitates [29], and locally laser-doped regions [30]–[34]. A technique was proposed by Nguyen *et al.* [35] to assess the doping level of a heavily-doped region by capturing the PL spectrum at low temperatures, courtesy of band-gap narrowing effects in heavily doped silicon [36]. In addition, micro-Raman spectroscopy can be used as a complementary technique to assess the local crystallinity and chemical components of the materials [37]–[40].

We first describe the processes involved in selectively depositing doped silicon by HWCVD, including tool conditions, liftoff lithography steps, and annealing steps. The characterization of the films is then undertaken using PL imaging, micro-PL spectroscopy and micro-Raman spectroscopy. The results are analyzed to provide key insights into the influence of decreasing silane flow rate, reducing annealing time, and depositing selectively over narrow areas. Micro-PL spectroscopy is then used to compare doping uniformity in selective area growth regions with that of doped regions formed by scanning, pulsed nanosecond laser doping.

II. EXPERIMENT

A. Process

P+ emitters are grown on 4" n-type wafers (FZ, 1–5 Ω-cm, $\langle 100 \rangle$, 280 μm) with a commercial HWCVD tool, which uses vapor-phase epitaxy, forming a doped epitaxial layer through chemical reactions between silane (SiH_4) and diborane (B_2H_6). The chamber pressure is set to 0.01 mbar, with wire and substrate temperatures of 2100 °C and 550 °C, respectively. The deposition time is fixed at 45 min. In this paper, silane/diborane flow rates (sccm) of 5/5, 10/10, and 20/20 are used to investigate the influence on crystallinity and defects. A 1/1 ratio is maintained between silane and diborane because of good rectification behavior observed for emitters grown with this ratio in previous work [11]. Furthermore, an investigation into selective growth of films over areas between 50 and 1000 μm in width is undertaken via lithography.

The process flow for selective growth is shown in Fig. 1. The substrate is first cleaned using piranha etch solution, and then briefly immersed in 1:20 HF solution. A 1-μm thick film of SiO_2 is grown using plasma enhanced chemical vapor deposition (PECVD) (14.5 min, SiH_4 = 4.2 sccm, N_2O = 350 sccm). Photolithography is then used to form openings for selective area growth, through the following steps: Spin on photoresist (AZ2070, 6000 r/min, 30 s), bake (110 °C, 60 s), expose (EVG620, 10 mW/ cm^2, 365 nm, 20 s), bake (110 °C, 60 s), develop (AZMIF726, 30 s), and then finally etch (13 min, 1:20 buffered HF). The finger openings are 1000, 500, 200, and 50 μm in width. The selective p+ emitters are then grown using the HWCVD tool (see above). A 1:7 buffered HF strip (30 min) is used to remove the remaining oxide layers, thereby lifting off the unwanted regions of HWCVD deposition. Postdeposition annealing treatments were undertaken in a tube furnace with an anneal temperature of 1000 °C for various times under N_2 gas flow.

Blanket test depositions (i.e., depositions over the whole wafer area, with no patterning) are also performed to study the effect of varying the annealing times from 1 to 4 h. The same deposition recipe as above is used. After annealing, these samples are passivated with a 17-nm layer of alumina by thermal atomic layer deposition (atomic layer deposition (ALD, Savannah 200). This provides both field effect and chemical passivation of the doped Si surface. Postdeposition annealing of the alumina film is undertaken for 30 min at 425 °C in forming gas consisting of hydrogen and argon to activate the surface passivation [41].

Laser-doped samples were fabricated on n-type substrates ($\sim$5 Ω-cm, 407 μm) with chemically etched surfaces. First, the sample undergoes a light damage etching process in 25% tetramethylammonium hydroxide (TMAH) solution at 80 °C for 5 min, followed by RCA cleaning. A spin-on-dopant layer made of B155 Poly boron spin-on dopant solution ($\sim$3 ml) from *Filmtronics* is then deposited using a spinner at 3000 r/min for 50 s. The dopant source layer is then baked at 90 °C for 20 min to remove solvents. A pulsed 532-nm fiber laser (23.1-μJ pulse energy, 600-ns duration with 50-kHz square waveform) is then used to drive in the dopants. Uniform exposure of 50-μm wide doped lines is achieved by overlapping the laser spot so that the pixel spacing is 6-μm (the laser spot has a diameter of 15 μm). Prior to the PL measurement, the sample surface is cleaned with standard RCA solution to remove the dopant source layer.

B. Characterization

The micro-PL/Raman spectroscopy system employed in this study is a Horiba LabRAM equipped with confocal optics. The incident laser light is focused onto the sample surface via a 50$\times$ objective lens with a numerical aperture of 0.55. The *XY* mapping stage has a minimum step size of 0.1 μm in both *X*- and *Y*- directions. Two excitation light sources were employed in this study: first, a diode-pumped solid-state 532-nm laser; and second, a supercontinuum NKT laser, whose emission wavelength is tuneable between 480 nm and 2 μm. A wavelength of 700 nm with a bandwidth of 10 nm was used in this study. The power was kept constant at 10 mW for all measurements. The illuminated spot size was $\sim$1 and $\sim$1.5 μm for the 532- nm and 700-nm excitation light sources, respectively. The sample temperature was regulated at 80 K by a liquid-nitrogen-cooled Linkam stage. The spectral response of the entire system was determined by a calibrated halogen–tungsten light source. For PL measurements, the emitted light was directed into a monochromator with a 150 grooves/mm grating, and then was detected by a liquid-nitrogen-cooled InGaAs array detector. For Raman measurements, a 1800 grooves/mm grating was used, and the detector was a silicon charge-coupled array device. Surface morphology was characterized using scanning electron microscopy (SEM, NVision40, Carl Zeiss). Lifetime was qualitatively measured using a PL imaging tool (BTi LIS-R1) with an excitation wavelength of 808 nm.
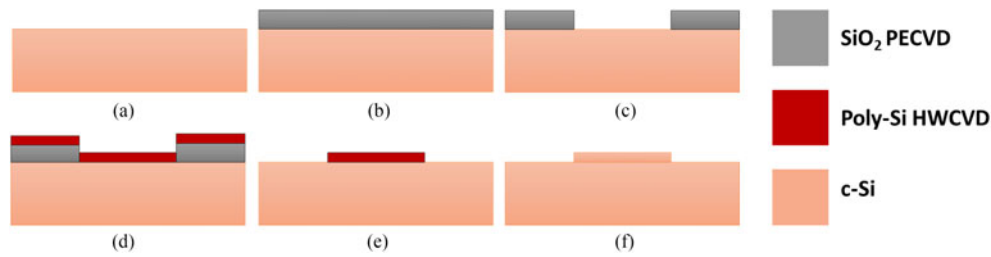
Fig. 1. Process flow for fabricating selectively-grown films in this paper (details in main text). (a) Cleaning step. (b) PECVD deposition of SiO_2. (c) Lithography to form opening. (d) HWCVD using silane and diborane gases. (e) Liftoff using wet etch. (f) Anneal using tube furnace.
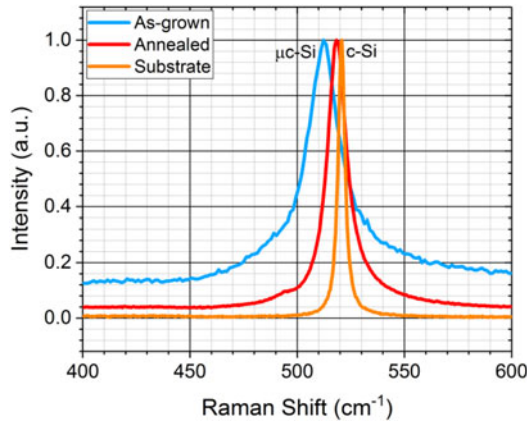

Fig. 2. Normalized Raman spectra captured from the as-grown (blue) and annealed (red) epitaxial regions for the 20/20 sccm silane /diborane HWCVD films. The Raman spectrum for the substrate (orange) is also shown.
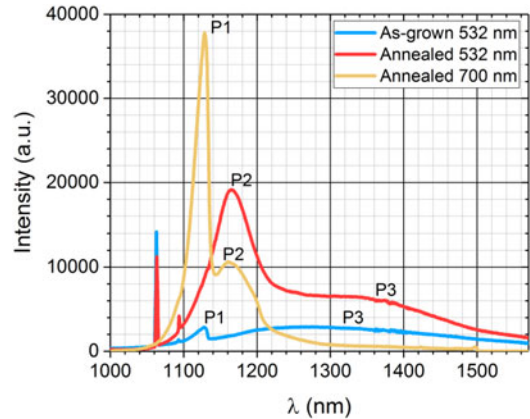

Fig. 3. PL spectra captured with 532-nm and 700-nm lasers at 80 K for samples produced by HWCVD deposition of boron-doped silicon onto silicon wafers with a 20/20 sccm silane/diborane flow rate. For the annealed samples, annealing was carried out at 1000 °C for 4 h.

III. RESULTS

A. 20/20 sccm Silane/diborane Ratio Films

Our previous work demonstrated that films grown with a silane/diborane ratio of 20/20 and then annealed for 4 h formed high-quality junctions with the potential for making high-efficiency solar cells [11]. Here, we first present further characterization of these films using Raman and PL spectroscopy. Fig. 2 shows Raman spectra captured from the as-grown (blue) and annealed (red) epitaxial regions. The spectrum from c-Si (orange) substrate is also included for comparison. A c-Si substrate gives a sharp Stoke-shift Raman peak at $\sim 520.7\,cm^{-1}$, whereas amorphous silicon (a-Si) gives a broad peak located around $\sim 480\,cm^{-1}$ [37]. The intermediate peak (located between c-Si peak and a-Si peak) is attributed to microcrystalline silicon (μc-Si), and its position and width are dependent on the grain size of the crystal [37], [38]. The Raman results indicate that the deposited film is crystallized by the 4-h anneal. The broader, more asymmetric and shifted c-Si Raman peak from the annealed epitaxial sample, compared with the substrate c-Si peak, is because of Fano resonance effects as a result of the high p-type doping concentration in the deposited film [40].

Fig. 3 shows the PL spectra for samples deposited using the 20/20 silane/diborane ratio, preanneal and postanneal. The figure also shows the PL spectra of the annealed sample using 532-nm and 700-nm excitation wavelengths. The PL peak P1 located ~ 1130 nm is the main band-to-band peak emitted from c-Si substrate. The PL peak P2 located at ~ 1165 nm is also

a band-to-band peak, but emitted from the heavily-doped p+ layer due to band-gap narrowing effects in heavily doped c-Si [36]. The broad peak P3 is attributed to subband-gap (defect) luminescence from the samples. In Fig. 3, the as-grown sample (blue curve) does not display a P2 peak (from p+ layer), whereas the annealed sample (red curve) exhibits a strong P2 peak. This supports the Raman results, confirming that the as-deposited film is not monocrystalline silicon, but then crystallizes after being annealed at 1000 °C for 4 h. Comparing spectra of 532-nm (red curve) and 700-nm (blue curve) excitation wavelengths, we see that the spectrum captured with 700-nm excitation light displays a strong P1 peak (from c-Si substrate), but reduced P2 (from p+ layer) and P3 (from defects) compared with that captured with 532-nm excitation light. This is because the longer wavelength light has a longer penetration depth and, thus, yields more PL signal from the underlying substrate but less PL signal from the top layer. These signatures indicate that the defect luminescence (P3) is emitted from either the epitaxial layer itself, or near the c-Si/epitaxial interface.

The increase of the P3 PL peak from as-grown to annealed samples under excitation at 532 nm is not associated with the crystallinity of the film (since crystallinity increases with annealing). The film undergoes densification during annealing, resulting in a thinner film and so an interface that is closer to the surface. The detected PL intensity from luminescent defects at the interface is therefore expected to be higher in the annealed sample due to less absorption of light in the thinner overlying
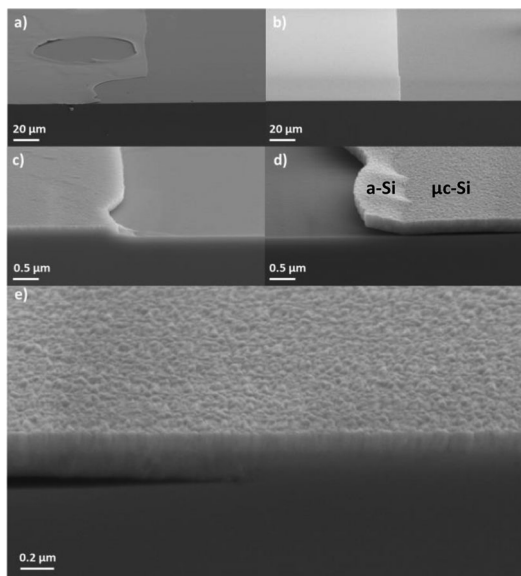
Fig. 4. SEM images of the annealed HWCVD films deposited with (a) and (c) 5/5 sccm, and (b), (d), and (e) 10/10 sccm silane/diborane flow rates. The tilt angle is 55°.
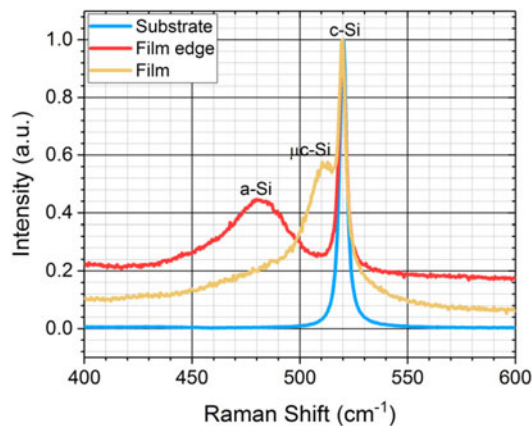

Fig. 5. Raman spectra for the as-deposited (before annealing) 10/10 sccm silane/diborane flow rate HWCVD films.
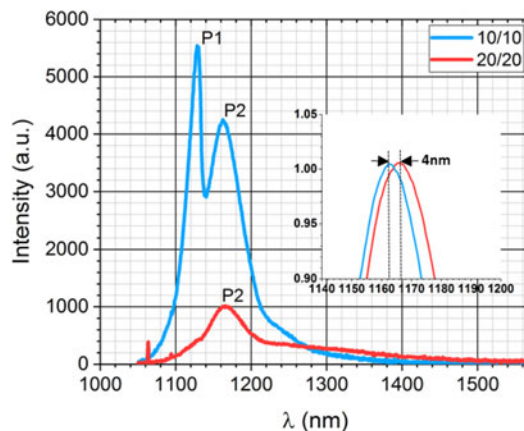

Fig. 6. PL spectra for 10/10 and 20/20 sccm silane/diborane flow rate HWCVD grown films, after annealing at 1000 °C for 4 h, captured with 532-nm laser at 80 K. Inset: Zoom on normalized P2 peaks for the two films, illustrating the shift in peak position.

silicon film. This could explain the increased P3 intensity of the red (annealed) curve compared with that of the blue (as-grown) curve in Fig. 3.

B. Reducing Silane Flow Rate

The PL study on the films grown with a silane/diborane ratio of 20/20 indicates the presence of luminescent defects (P3 peak) associated with the interface between the substrate and deposited film. For solar cell applications, these defects could be detrimental to performance as they are likely to increase the recombination of minority carriers. In an effort to reduce the number of these defects at the interface, experiments were carried out with lower gas flow rates of 5/5 and 10/10 sccm. It is expected that lower flow rates will provide more time for Si atoms to diffuse on the surface and find the lowest energy sites, hence reducing defect density.

1) Morphology: SEM images of freshly cleaved samples, as presented in Fig. 4, show the annealed films, deposited under the conditions of 5/5 and 10/10 sccm silane/diborane flow rates. Imaging the deposited films at low magnification shows the poor uniformity of the 5/5 deposition [see Fig. 4(a)], with large holes appearing across the selective region. The nonuniformity can be attributed to the low silane flow rate, which prevents the uniform formation of seed layers. As such, this flow rate is not suitable for the formation of continuous emitters needed for an efficient IBC solar cell. However, the 10/10 ratio is shown to form continuous films throughout the selective regions [see Fig. 4(b)]. At higher magnification [see Fig. 4(c) and (d)], the film shows signs of delamination at the edge. It is suggested that this is a result of deposition of silicon onto the edges of the oxide mask, in the form of amorphous silicon (as confirmed by Raman measurements, Fig. 5), and thus, causes ineffective masking for the liftoff process. A workaround to this in future processing will be to use an additional sacrificial nitride layer to form an undercut thereby ensuring that there is separation between Si grown on

substrate and Si grown on mask. Fig. 4(e) shows the cross section of 10/10 film at even higher magnification, illustrating the roughness of the film and the uniform interface with the substrate away from the edge, which could be attributed to the formation of μc-Si instead of a continuous epitaxial layer. SEM images and profiler measurements (not presented) show the 10/10 film to be 350 nm thick, which is approximately half the thickness of the films deposited using 20/20 sccm silane/diborane flow rates shown in a previous work [11].

Fig. 5 shows Raman spectra (before annealing) of the film deposited over a selective area using a 10/10 sccm silane/diborane ratio. The Raman spectra show that the 10/10 film is μc-Si, but at the edge there is an a-Si region, which is due to deposition occurring on the edges of the oxide mask prior to liftoff. Note that the underlying substrate peak is visible in all spectra for the 10/10 film, whereas it is not present in the Raman spectrum for the 20/20 film (Fig. 2, blue line). This is due to the slower growth rate that results in the 10/10 film having approximately half the thickness of the 20/20 film, allowing the Raman signal from the underlying substrate to be detected.

2) Luminescent Defects: Fig. 6 shows the PL spectra for the films deposited over selective areas using 10/10 and
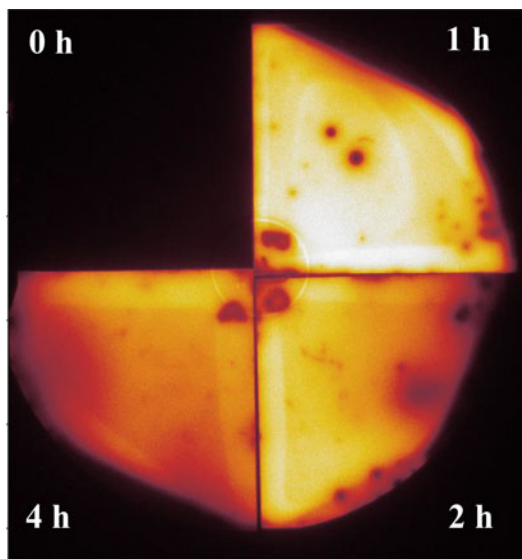
Fig. 7. PL image of 10/10 sccm silane/diborane flow rate HWCVD films annealed for different times at 1000 °C. The brighter color indicates the higher PL intensity and therefore higher effective carrier lifetime.
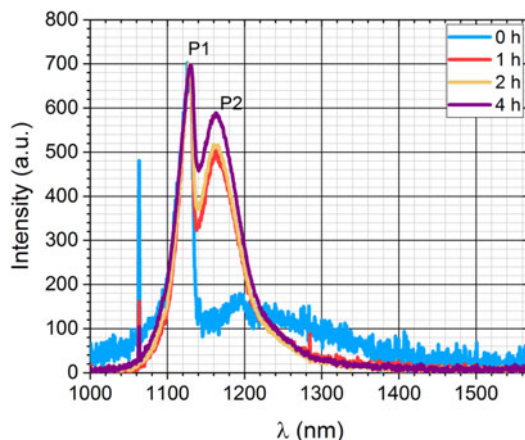

Fig. 8. PL spectra for 10/10 sccm silane/diborane flow rate HWCVD film annealed for different annealing times at 1000 °C, captured with the 532-nm laser at 80 K and normalized to the P1 peak.

20/20 sccm silane/diborane ratios, after annealing for 4 h at 1000 °C. The spectra were captured from the middle of the deposited areas to avoid the amorphous regions at the edges. A clear reduction in luminescent defects (P3) is observed when reducing the silane flow rate to 10/10. The quality of an epitaxial layer is determined by the nature of the surface prior to epitaxial growth as well as the arrival rate relative to the surface diffusion rate [42]. In this case, the reduced silane rate provides a longer time for Si atoms to diffuse and find the lowest energy sites and thereby reduce the number of crystal defects that occurs during growth, which leads to a smaller P3 peak. The P2 peak emitted from the p+ layer of the 10/10 sample is shifted ∼4 nm to the shorter wavelength side compared with the 20/20 sample, and its intensity is less pronounced compared with the main band-to-band peak (P1) than for the 20/20 sample. As recently reported by Han *et al.* [43], the position of the peak emitted from the boron-diffused layer is strongly correlated with the surface dopant density, whereas the relative intensity (compared with the main band-to-band peak) is correlated with the diffusion thickness (characterized by the depth factor in their work). The annealed epitaxial layers in this study are, in principle, similar to the diffusion process (a layer with very high concentration of boron was deposited and annealed to drive in the dopant atoms). Therefore, the 4-nm shifting indicates that the p+ layer of the 10/10 sample has a lower surface dopant density than the 20/20 sample [35]. The band-to-band peak (P1) is barely visible in the 20/20 sample, which, in addition to the higher doping level, is thought to be due to the film being thicker (and therefore the signal from the underlying substrate being therefore smaller) as well as being of lower quality (more defective).

3) Effect of Anneal Time: Our previously reported work on films deposited with 20/20 sccm silane/diborane flow rates revealed an increasing lifetime with increasing anneal time up to 4 h [11]. Fig. 7 shows PL images taken at room temperature of the band-to-band luminescence from samples with blanket-deposited and passivated films with 10/10 sccm silane/diborane flow rates for various annealing times. Note that the as-deposited sample is invisible in Fig. 7 (upper-left corner) due to its extremely low PL intensity. These images show that the effective lifetime is significantly boosted with a 1-h anneal, and decreases with further annealing, which indicates that the optimum anneal time is much shorter for the 10/10 film compared with the 20/20 film. This may be because the reduced silane flow rate leads to improved crystallinity of the as-deposited film and therefore full crystallization can be achieved with a shorter anneal time. This is further supported by Fig. 8, which shows significant reduction in the luminescent defect peak (P3) after annealing for 1 h. All annealed samples exhibit a P2 peak, indicating good crystallinity, but longer anneal times are thought to reduce lifetime due to deeper junction formation as well as drive in of any contaminants during processing. Note that the difference in thicknesses of the films may also have an effect, increasing the time required for the thicker 20/20 film to fully crystallize.

C. Selective Area Width

The results in the previous sections demonstrate that reducing the gas flow rate to 10/10 sccm silane/diborane reduces the number of luminescent defects present at the interface between the deposited film and substrate. Furthermore, a shorter anneal time is required to crystallize the film deposited at the lower gas flow rate and improve the effective carrier lifetime. However, for application as a method of forming emitter fingers on IBC cells, film quality must be maintained when depositing over narrow selective areas.

Fig. 9 shows the PL spectra for films deposited using a 10/10 sccm silane/diborane ratio, selectively grown with various emitter widths and then annealed (for 4 h at 1000 °C). The reduction in the width has very little impact on the PL spectra and therefore the quality of the film, with results that indicate a low defect density (negligible P3 peak) for all measurements. This is encouraging for application in an IBC process, where
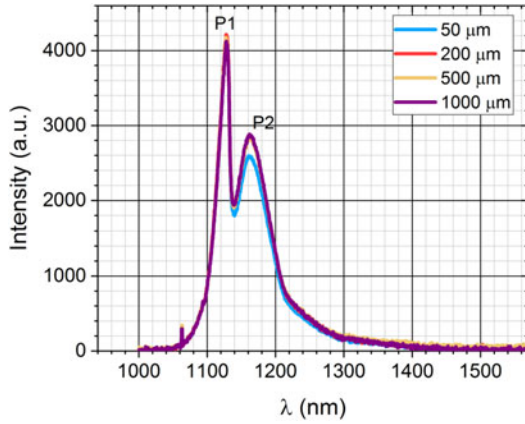
Fig. 9. PL spectra of films, deposited over various selective area widths using a 10/10 sccm silane/diborane ratio and annealed for 4 h at 1000 °C. The spectra were captured using excitation from the 532-nm laser at 80 K from the middle of each deposited area to avoid the a-Si regions at the edges.
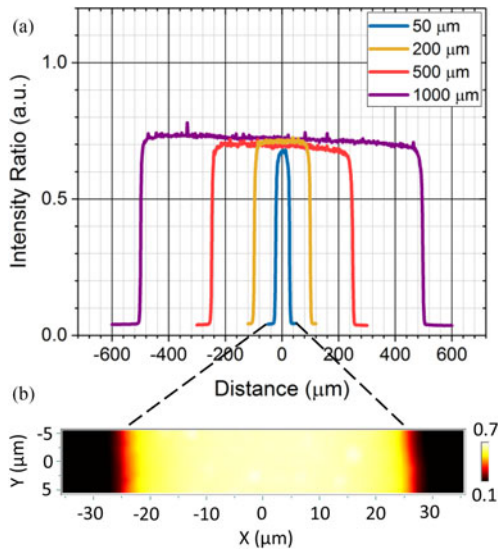

Fig. 10. (a) PL intensity ratio, between P2 peak (emitted from the p+ layer) and P1 peak (emitted from the c-Si substrate) qualitatively representing the doping density of the p+ layer. (b) Two-dimensional map of PL intensity ratio of the 50-μm finger width, excited with the 532-nm laser at 80 K.
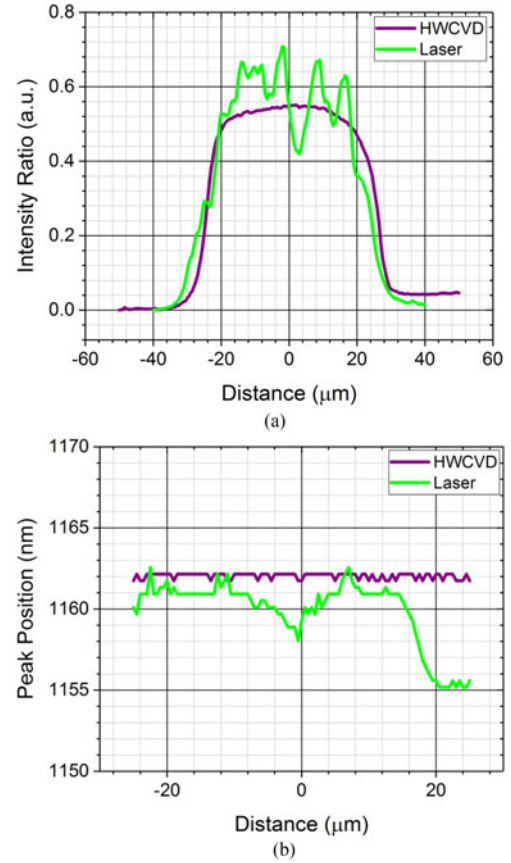

Fig. 11. Comparison of lateral doping uniformity of HWCVD process and Laser-doped process, using PL intensity ratio (P2/P1) (a) and PL P2 peak position (b) excited with the 532-nm laser at 80 K.

observable when comparing both PL intensity ratio and PL P2 peak position.

IV. CONCLUSION

Doped silicon films grown on selective areas of silicon wafers by HWCVD have been characterized with a view to using the technique as a low-cost alternative to forming diffused emitters in all back contact silicon solar cells. Morphology and Raman spectroscopy analysis has shown that nonuniform films are grown when using a very low silane flow rate (5 sccm). By doubling this flow rate, uniform microcrystalline films are grown. A further doubling of this flow rate maintains film uniformity but reduces the crystallinity and increases the defect concentration (determined using spectral PL measurements). Through utilizing two different lasers for the PL spectral analysis, the dominant site for defects was identified as near the interface between the grown layer and substrate. Selective growth of the epitaxial fingers showed no reduction in crystallinity or increase in defect intensity when reduced to 50 μm width. Furthermore, PL spectral line scans showed that sharp doping profiles, uniform across the deposited area, are maintained for the various selective growth widths. Reducing the silane rate also results in shorter anneal times required for crystallization and therefore potentially a low thermal budget when used in cell fabrication. In going forward, further studies need to be under-

the selective growth of emitters of these feature sizes is a key requirement. Furthermore, PL line scans (see Fig. 10) illustrate the sharpness of the edges of the selective area deposits, which indicates that the growth and postanneal processes do not impact the surrounding material. The line scans in Fig. 10(a) are plotted as the intensity ratio of the P1 and P2 peaks at each point (P2/P1), which correlates with doping level, as reported in [35], [43]. The results show that the doping is maintained strictly within the epitaxial regions and that lateral diffusion and other edge effects are minimal. The lateral uniformity in the diffusion profile is highlighted in the two-dimensional map in Fig. 10(b), and is shown to be better than that of laser doping in Fig. 11. The latter process suffers from nonuniformity due to the close overlapping of laser pulses, which have a Gaussian spatial distribution in energy density [44], [45]. This nonuniformity is

taken in the following areas: Optimization of the anneal time and temperature to further reduce the thermal budget; introduction of a heated stage to increase substrate temperature during growth with the aim of negating the need for a postgrowth anneal; and optimization of the thickness of the deposited film and pretreatment of the wafer surface prior to HWCVD.

ACKNOWLEDGMENT

REFERENCES

[1] K. Yoshikawa *et al.*, "Silicon heterojunction solar cell with interdigitated back contacts for a photoconversion efficiency over 26%," *Nature Energy*, vol. 2, 2017, Art. no. 17032.

[2] T. Rahman *et al.*, "Passivation of all-angle black surfaces for silicon solar cells," *Solar Energy Mater. Solar Cells*, vol. 160, pp. 444–453, 2017.

[3] T. Rahman, M. Navarro-Cía, and K. Fobelets, "High density micropyramids with silicon nanowire array for photovoltaic applications," *Nanotechnology*, vol. 25, no. 48, 2014, Art. no. 485202.

[4] E. Franklin *et al.*, "Design, fabrication and characterisation of a 24.4% efficient interdigitated back contact solar cell," *Prog. Photovolt.*, vol. 24, no. 4, pp. 411–427, 2016.

[5] T. Rahman *et al.*, "Minimising bulk lifetime degradation during the processing of interdigitated back contact silicon solar cells," *Prog. Photovolt., Res. Appl.*, vol. 26, no. 1, pp. 38–47, 2018.

[6] N. Bateman *et al.*, "High quality ion implanted boron emitters in an interdigitated back contact solar cell with 20% efficiency," *Energy Procedia*, vol. 8, pp. 509–514, 2011.

[7] M. Dahlinger *et al.*, "23.2% laser processed back contact solar cell: fabrication, characterization and modeling," *Progress Photovolt., Res. Appl.*, vol. 25, no. 2, pp. 192–200, 2017.

[8] M. Ernst *et al.*, "Fabrication of a 22.8% efficient back contact solar cell with localized laser-doping," *Physica Status Solidi (a)*, vol. 214, no. 11, 2017, Art. no. 1700318.

[9] M. R. Payo *et al.*, "Boron-doped selective silicon epitaxy: High efficiency and process simplification in interdigitated back contact cells," *Prog. Photovolt., Res. Appl.*, vol. 22, no. 7, pp. 711–725, 2014.

[10] T. Rachow *et al.*, "Solar cells with epitaxial or gas phase diffused emitters above 21% efficiency," *Energy Procedia*, vol. 77, pp. 540–545, 2015.

[11] T. Rahman *et al.*, "Junction formation with HWCVD and TCAD model of an epitaxial back-contact solar cell," *IEEE J. Photovolt.*, vol. 6, no. 6, pp. 1396–1402, Nov. 2016.

[12] T. Trupke, R. Bardos, and M. Abbott, "Self-consistent calibration of photoluminescence and photoconductance lifetime measurements," *Appl. Phys. Lett.*, vol. 87, no. 18, 2005, Art. no. 184102.

[13] T. Trupke *et al.*, "Photoluminescence imaging of silicon wafers," *Appl. Phys. Lett.*, vol. 89, no. 4, 2006, Art. no. 044107.

[14] T. Mchedlidze *et al.*, "Capability of photoluminescence for characterization of multi-crystalline silicon," *J. Appl. Phys.*, vol. 111, no. 7, 2012, Art. no. 073504.

[15] E. Daub and P. Würfel, "Ultralow values of the absorption coefficient of Si obtained from luminescence," *Phys. Rev. Lett.*, vol. 74, no. 6, 1995, Art. no. 1020.

[16] T. Trupke *et al.*, "Temperature dependence of the radiative recombination coefficient of intrinsic crystalline silicon," *J. Appl. Phys.*, vol. 94, no. 8, pp. 4930–4937, 2003.

[17] H. T. Nguyen *et al.*, "Temperature dependence of the band-band absorption coefficient in crystalline silicon from photoluminescence," *J. Appl. Phys.*, vol. 115, no. 4, 2014, Art. no. 043710.

[18] P. Altermatt *et al.*, "Injection dependence of spontaneous radiative recombination in crystalline silicon: Experimental verification and theoretical analysis," *Appl. Phys. Lett.*, vol. 88, no. 26, 2006, Art. no. 261901.

[19] H. T. Nguyen, S. C. Baker-Finch, and D. Macdonald, "Temperature dependence of the radiative recombination coefficient in crystalline silicon from spectral photoluminescence," *Appl. Phys. Lett.*, vol. 104, no. 11, 2014, Art. no. 112105.

[20] C. Barugkin *et al.*, "Evaluating plasmonic light trapping with photoluminescence," *IEEE J. Photovolt.*, vol. 3, no. 4, pp. 1292–1297, Oct. 2013.

[21] P. Würfel *et al.*, "Diffusion lengths of silicon solar cells from luminescence images," *J. Appl. Phys.*, vol. 101, no. 12, 2007, Art. no. 123110.

[22] J. Giesecke *et al.*, "Separation of local bulk and surface recombination in crystalline silicon from luminescence reabsorption," *Progress Photovolt., Res. Appl.*, vol. 18, no. 1, pp. 10–19, 2010.

[23] M. P. Peloso *et al.*, "Evaluating the electrical properties of silicon wafer solar cells using hyperspectral imaging of luminescence," *Appl. Phys. Lett.*, vol. 99, no. 22, 2011, Art. no. 221915.

[24] B. Mitchell *et al.*, "Bulk minority carrier lifetimes and doping of silicon bricks from photoluminescence intensity ratios," *J Appl. Phys.*, vol. 109, no. 8, 2011, Art. no. 083111.

[25] B. Mitchell *et al.*, "Full spectrum photoluminescence lifetime analyses on silicon bricks," *IEEE J. Photovolt.*, vol. 3, no. 3, pp. 962–969, Jul. 2013.

[26] M. Tajima *et al.*, "Deep-level photoluminescence due to dislocations and oxygen precipitates in multicrystalline Si," *J. Appl. Phys.*, vol. 111, no. 11, 2012, Art. no. 113523.

[27] M. Tajima, "Spectroscopy and topography of deep-level luminescence in photovoltaic silicon," *IEEE J. Photovolt.*, vol. 4, no. 6, pp. 1452–1458, Nov. 2014.

[28] P. Gundel *et al.*, "Quantitative carrier lifetime measurement with micron resolution," *J. Appl. Phys.*, vol. 108, no. 3, 2010, Art. no. 033705.

[29] P. Gundel *et al.*, "Micro-photoluminescence spectroscopy on metal precipitates in silicon," *Phys. Status Solidi Rapid Res. Lett.*, vol. 3, no. 7–8, pp. 230–232, 2009.

[30] R. Woehl *et al.*, "Evaluating the aluminum-alloyed p+ layer of silicon solar cells by emitter saturation current density and optical microspectroscopy measurements," *IEEE Trans. Electron Devices*, vol. 58, no. 2, pp. 441–447, Feb. 2011.

[31] P. Gundel *et al.*, "Comprehensive microscopic analysis of laser-induced high doping regions in silicon," *IEEE Trans. Electron Devices*, vol. 58, no. 9, pp. 2874–2877, Sep. 2011.

[32] F. D. Heinz *et al.*, "Doping density in silicon and solar cells analyzed with micrometer resolution," *IEEE J. Photovolt.*, vol. 3, no. 1, pp. 341–347, Jan. 2013.

[33] A. Roigé *et al.*, "Microscale spatially resolved characterization of highly doped regions in laser-fired contacts for high-efficiency crystalline Si solar cells," *IEEE J. Photovolt.*, vol. 5, no. 2, pp. 545–551, Mar. 2015.

[34] H. T. Nguyen *et al.*, "Dislocations in laser-doped silicon detected by microphotoluminescence spectroscopy," *Appl. Phys. Lett.*, vol. 107, no. 2, 2015, Art. no. 022101.

[35] H. T. Nguyen *et al.*, "Micro-photoluminescence spectroscopy on heavily-doped layers of silicon solar cells," *Physica Status Solidi Rapid Res. Lett.*, vol. 9, no. 4, pp. 230–235, 2015.

[36] J. Wagner, "Band-gap narrowing in heavily doped silicon at 20 and 300 K studied by photoluminescence," *Phys. Rev. B*, vol. 32, no. 2, 1985, Art. no. 1323.

[37] D. Bermejo and M. Cardona, "Raman scattering in pure and hydrogenated amorphous germanium and silicon," *J. Non-Crystalline Solids*, vol. 32, no. 1-3, pp. 405–419, 1979.

[38] Z. Iqbal *et al.*, "Raman scattering from small particle size polycrystalline silicon," *Solid State Commun.*, vol. 37, no. 12, pp. 993–996, 1981.

[39] F. Heinz, W. Warta, and M. Schubert, "Optimizing micro Raman and PL spectroscopy for solar cell technological assessment," *Energy Procedia*, vol. 27, pp. 208–213, 2012.

[40] T. Kunz *et al.*, "Dopant mapping in highly p-doped silicon by micro-Raman spectroscopy at various injection levels," *J. Appl. Phys.*, vol. 113, no. 2, 2013, Art. no. 023514.

[41] W. Liang *et al.*, "Surface passivation of boron-diffused p-Type silicon surfaces with (1 0 0) and (1 1 1) orientations by ALD Al_2O_3 layers," *IEEE J. Photovolt.*, vol. 3, no. 2, pp. 678–683, Apr. 2013.

[42] M. L. Hammond, "2 - Silicon epitaxy by chemical vapor deposition A2-Seshan, Krisna," in *Handbook of Thin Film Deposition Processes and Techniques*, 2nd ed. Norwich, NY, USA: William Andrew Publ., 2001, pp. 45–110.

[43] Y.-J. Han *et al.*, "Determination of dopant density profiles of heavily boron-doped silicon from low temperature microphotoluminescence spectroscopy," *IEEE J. Photovolt.*, vol. 7, no. 6, pp. 1693–1700, Nov. 2017.

[44] M. H. Norouzi *et al.*, "Development and characterization of AlO_x/SiN_x: B Layer systems for surface passivation and local laser doping," *IEEE J. Photovolt.*, vol. 7, no. 5, pp. 1244–1253, Sep. 2017.

[45] A. Roige *et al.*, "Effects of photon reabsorption phenomena in confocal micro-photoluminescence measurements in crystalline silicon," *J. Appl. Phys.*, vol. 121, no. 6, 2017, Art. no. 063101.